

# BL33XU TOYOTA

## 1. Introduction

The BL33XU, the Toyota beamline, was built in FY2009 and is operated by Toyota Central R&D Labs., Inc. [1]. The original purpose of this beamline was to perform quick-scanning X-ray absorption spectroscopy (QXAFS) for *operando* analysis and three-dimensional X-ray diffraction (3DXRD). These techniques were not available at SPring-8 before 2009 and were needed for industrial applications. In addition to these, the following techniques have been adopted: X-ray diffraction (XRD), X-ray computed tomography (CT)/laminography, and small-angle X-ray scattering (SAXS) as shown in Fig. 1. In this report, we describe the current status of this beamline and recent technical progress.

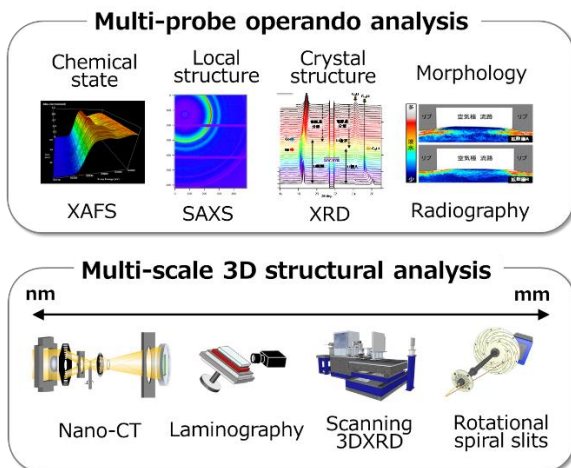


Fig. 1. Measurement techniques at BL33XU.

## 2. BL33XU beamline

### 2-1. Beamline layout

The medium-length beamline BL33XU has the optics hutch in the storage ring building of SPring-8. The experimental facility building is located

outside the storage ring building. The building has three experimental hutches, a chemical laboratory, and an office room.

The layout of the optical components of BL33XU is shown in Fig. 2, where two different types of monochromator are installed. Optics 1 is mainly used for QXAFS. It is composed of horizontal deflection mirrors (M1 and M2) in the optics hutch, compact monochromators (C-Mono) with channel-cut crystals, and vertical deflection mirrors (M3 and M4) in the experimental hutch 1. Optics 2 is used for 3DXRD and other techniques. It consists of a SPring-8 standard double-crystal monochromator, vertical deflection mirrors (M4 and M5), and Kirkpatrick–Baez focusing mirrors (KBMs) that yield a  $1 \mu\text{m}^2$  microbeam at 50 keV in experimental hutch 3.

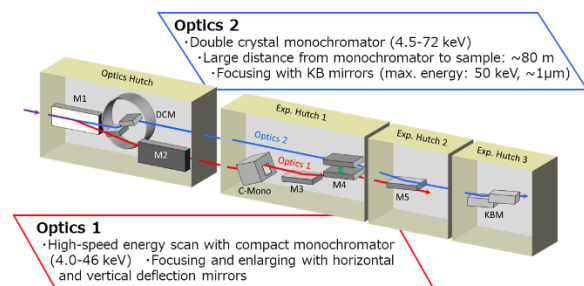


Fig. 2. Optical components of BL33XU.

## 2-2. Analysis techniques

### (1) QXAFS

A tapered undulator combined with the servo-motor-driven channel-cut monochromator realizes the rapid data acquisition of XAFS with a temporal resolution of 10 ms [2]. The energy range from 4.0 to 45 keV is accomplished by the two monochromators with Si(111) and Si(220) crystals.

This QXAFS system has enabled the development of various *in situ* measurement techniques such as simultaneous XAFS and XRD measurements of positive and negative electrodes of lithium-ion batteries during charging and discharging [3].

### (2) SAXS

The camera distance from tens of centimeters to 4.5 meters can be selected for SAXS at BL33XU. A two-dimensional detector, PILATUS 300K (Dectris), is available for the developed *in situ* measurement system. An example is an *in situ* measurement to analyze the structural evolution of resins during injection molding [4].

### (3) XRD

For the analysis of the reliability of mechanical and electronic components, it is important to measure the internal stresses and strains nondestructively. The measurement based on XRD was realized by a multi-axial goniometer equipped with a newly developed rotating and revolving spiral slit system. The rotating shield disks with the slits enable the detection of diffraction only from a small gage volume of interest inside a component with a two-dimensional detector, PILATUS. This system realizes the depth-resolved distribution measurement of strains in an actual mechanical component [5].

### (4) Scanning 3DXRD

To measure the three-dimensional distribution of stresses inside the grains of a bulk sample, i.e., type III stresses, the scanning three-dimensional X-ray diffraction (3DXRD) microscopy methodology was developed [6]. This nondestructive technique was validated in 2013, and the three-dimensional distribution of stresses inside the grains of bulk polycrystalline steel under tensile deformation was measured in 2019 [7]. The results revealed that the

microscopic intragranular stresses greatly deviate from the macroscopic average stresses measured by conventional methods. Combined with other nondestructive measurement techniques such as XRD and laminography, 3DXRD is expected to facilitate the development of multi-scale material modeling that expresses the deformation, fracture, and life of components.

### (5) X-ray CT and laminography

To meet the growing needs for the high-resolution nondestructive observation of internal behavior in mechanical and electronic components, X-ray computed tomography and laminography techniques were introduced. The resolutions of the two imaging techniques are less than 1  $\mu\text{m}$  even under *in situ* measurement where sample materials and components are exposed to actual working conditions. The newly adopted CT system with a Fresnel zone plate (FZP) has achieved a resolution of  $\sim 100$  nm.

## 3. Recent technological progress: Crystal structure analysis near interfaces in solid oxide fuel cells (SOFCs) by microbeam XRD for reduction in environmental load

SOFCs are composed of ceramics that enable operation at temperatures above 700°C to yield a high electricity generation efficiency than other kinds of fuel cells. The improvement of cell durability is expected to accelerate the spread of SOFCs in society and consequently contribute to the reduction in environmental load. For the realization of SOFCs, an understanding of the microscopic composition, crystal structures, and byproducts of the electrodes, electrolyte, and their interfaces is important. A microbeam X-ray diffraction technique was developed at BL33X to

realize the high-spatial-resolution measurement of the crystal structure and phases near the interfaces of SOFCs [8].

X-rays of 50 keV, monochromatized by a Si311 monochromator, were focused to make a 1  $\mu\text{m}$  by 1  $\mu\text{m}$  microbeam using the K-B mirror and irradiated onto the sample surface at an incident angle of  $1.5^\circ$  as shown in Fig. 3. The X-ray diffraction pattern was measured by a two-dimensional detector (Pilatus-300K) placed at a distance of about 500 mm from the sample. The sample was moved in the direction of cell thickness in 1  $\mu\text{m}$  steps, and X-ray diffraction measurements were performed for 150 s at each point.

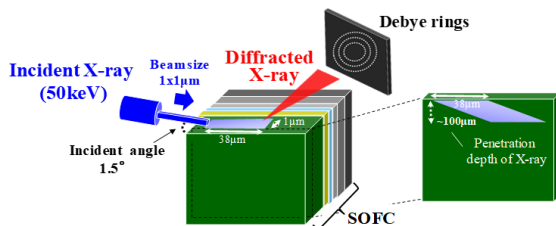


Fig. 3. Schematic of microbeam X-ray diffraction measurement of SOFC cells.

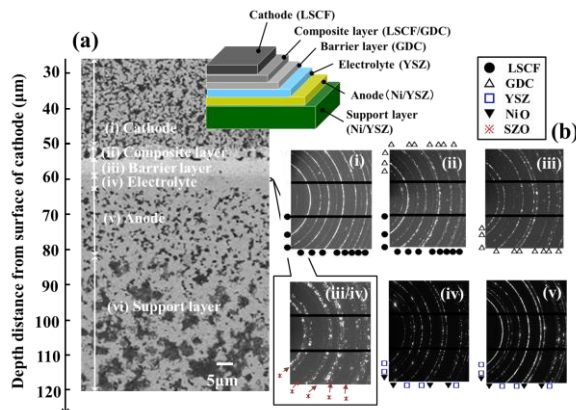


Fig. 4. Microstructure of SOFC sample: (a) cross-sectional image obtained by scanning electron microscopy (SEM) and (b) X-ray diffraction pattern of each layer.

A SOFC coin cell was cut and the cross section was mirror-polished to obtain the measurement surface. The electrode is composed of a cathode, an interface layer, electrolyte, an anode, and a support layer as shown in Fig. 4(a), where LSCF is  $(\text{La,Sr})(\text{Co,Fe})\text{O}_3$ , GDC is  $(\text{Gd,Ce})\text{O}_2$ , and YSZ is Y-stabilized  $\text{ZrO}_2$ . The X-ray diffraction pattern of each layer is shown in Fig. 4(b). It was found that even layers only a few micrometers thick can be identified by the microbeam XRD technique developed at BL33XU.

Figures 5(a) and 5(b) respectively show the XRD and SEM results of the barrier layer, electrolyte, and their interfaces. It was confirmed that  $\text{CeO}_2\text{-ZrO}_2$  was created by the reaction between GDC and YSZ at the interface between the barrier layer and the electrolyte.  $\text{SrZrO}_3$  (SZO) was also observed at the interface owing to the reaction between Sr and YSZ.

Figures 5(c) and 5(d) show the changes in the lattice parameter of YSZ from the electrolyte to the support layer. These changes in the lattice parameter are due to the change in the amount of Y doping. Near the interface of each layer, the changes are continuous owing to the interdiffusion of Y in each layer.

These results show that it is possible to visualize the crystal structure change and byproduct phases at micron order in the direction of the SOFC cell cross section. This technique will be useful for the development of high-efficiency fuel cells that will contribute to the reduction in environmental load.

Hidehiko Kimura and Hiroshi Nozaki

Toyota Central R&D Labs

## References:

- [1] Nonaka, T. et al. (2016). *AIP Conf. Proc.* **1741**, 030043.
- [2] Nonaka, T. et al. (2012). *Rev. Sci. Instrum.* **83**, 083112.
- [3] Makimura, Y. et al. (2016). *J. Electrochem. Soc.* **163**(7), A1450-A1456.
- [4] Harada, M. et al. (2015). *SPring-8 User Experiment Report*, 2015A7003, 2015B7003.
- [5] Setoyama, D. et al. (2015). *Proc. MECASENSE 2015*, 4.
- [6] Hayashi, Y. et al. (2017). *SPring-8 User Experiment Report* 2017A7002, 2017B7002.
- [7] Hayashi, Y. et al. (2019). *Science* **366**, 1492–1496.
- [8] Nozaki, H. et al. (2021). *Mater. Lett.* **277**, 128383.

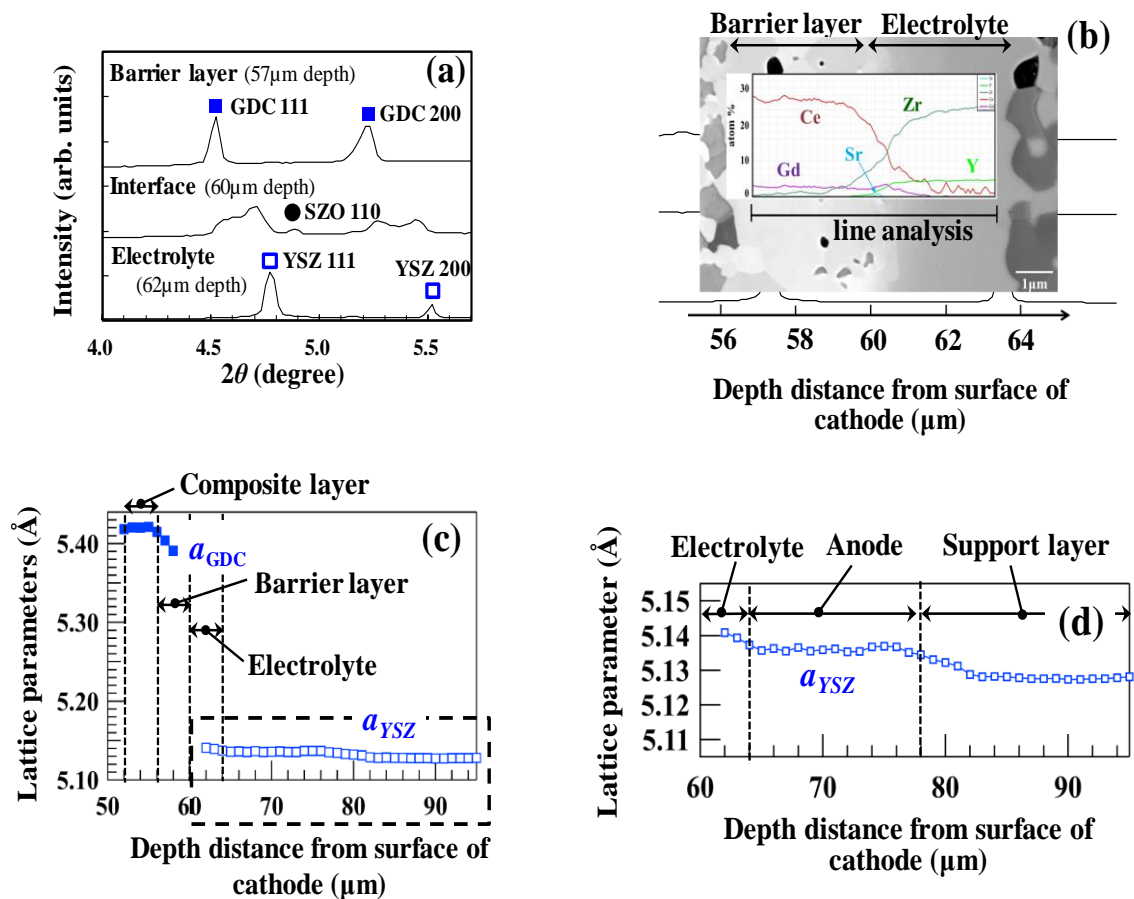


Fig. 5. Microbeam measurement results: (a) XRD patterns, (b) SEM image, (c) lattice parameter changes near the interface, and (d) magnification of dashed square in (c).